**Nak-Kyun Cho**
Department of Mechanical & Aerospace Engineering,
University of Strathclyde,
Glasgow G1 1XJ, UK

**Haofeng Chen**
Department of Mechanical & Aerospace Engineering,
University of Strathclyde,
Glasgow G1 1XJ, UK;
School of Mechanical and Power Engineering,
East China University of Science and Technology,
Shanghai Shi 200237, China
e-mail: haofeng.chen@strath.ac.uk

**Donald Mackenzie**
Department of Mechanical & Aerospace Engineering,
University of Strathclyde,
Glasgow G1 1XJ, UK

**Dario Giugliano**
Department of Mechanical & Aerospace Engineering,
University of Strathclyde,
Glasgow G1 1XJ, UK;
School of Mechanical and Power Engineering,
East China University of Science and Technology,
Shanghai Shi 200237, China

# Investigating the Effects of Cyclic Thermo-Mechanical Loading on Cyclic Plastic Behavior of a Ninety-Degree Back-to-Back Pipe Bend System

*Pipe bends are generally employed for routing piping systems by connecting to straight pipes but back-to-back pipe bends are often necessary for confined space applications. In order to achieve safe operation under complex loading, it requires a thorough pipeline integrity assessment to be commenced. This paper investigates the effects of cyclic thermo-mechanical loading on cyclic plastic behavior of a 90-deg back-to-back pipe bend system, including temperature-dependent yield stress effects. Structural response interaction boundaries are determined for various different combinations of cyclic and steady loading. Constructed structural responses are verified by full cyclic incremental, step-by-step, finite element analysis. The numerical studies provide a comprehensive description of the cyclic plastic behavior of the pipe bends, and semi-empirical equations for predicting the elastic shakedown limit boundary are developed to aid pipeline designers in the effective assessment of the integrity of the pipe bends without a requirement for complex finite element analysis.* [DOI: 10.1115/1.4043376]

*Keywords: pipe bends, shakedown, ratcheting, cyclic thermo-mechanical load*

## 1 Introduction

Power plant piping systems are designed to avoid plastic collapse under monotonic loading and low cycle fatigue and ratcheting failures under cyclic loading. Piping systems are mainly composed of straight pipe and pipe bend components. Pipe bends are generally employed for routing piping systems by connecting to straight pipes but back-to-back pipe bends are often necessary components in confined space applications. Structural integrity assessment of pipe bends is more complex than for a straight pipeline [1–3]. Also, the high temperature operating condition causes the material degradation of the pipe bends, such as the reduction of yield stress under cyclic loading condition, which leads to low cycle fatigue failure or ratcheting failure. It is, therefore, necessary to consider the effects of temperature-dependent yield on the pipe bend integrity assessment. Structural integrity assessment under cyclic loadings is an important feature in a wide range of engineering applications and many types of research have reported cyclic plasticity behavior of engineering problems [4–7].

The full incremental cyclic analysis using the finite element method is commonly employed to determine the cyclic plasticity responses of components subjected to a variety of load combination. However, conventional finite element analysis evaluates the structural response for a specific cyclic loading condition. To construct response boundaries, such as the shakedown and ratchet limits, a significant number of trial loading conditions must be considered. This usually requires an extensive computational resource, in particular for complex three-dimensional (3D) geometries. Several direct methods have been developed to reduce computational requirements and directly determine the structural response in the form of a Bree diagram [8]. The representative direct methods include the gloss R-node method [9], the elastic compensation method, Dhalla reduction procedure [10], and the linear matching method (LMM) [11]. Chen and Ponter extended the scope of the LMM to include ratchet limit analysis, creep rupture limit analysis, and cyclic plasticity analysis which considers creep-fatigue interaction [12,13], and the whole extended analysis package is called the LMM framework.

The cyclic plasticity of several types of pipe geometry under cyclic loading had been studied before [14–19]. However, no research has been presented for the cyclic plasticity response of the pipe geometry in the subject under thermo-mechanical load with temperature dependent material properties. This paper presents the results of a detailed investigation cyclic plastic behavior of the pipe bends under cyclic out-of-plane bending and cyclic thermal load with steady internal pressure. Two types of the double pipe bend systems are adopted: the one has two single elbows directly connected to each other and the other one has an additional straight pipe run between the elbows. The former one is the main geometry and the latter is used for parametric studies.

An overview of the LMM framework and its numerical procedures are presented in Sec. 2. Section 3 provides the problem descriptions which include the finite element model of the pipe bend configuration and the applied loading condition. The numerical results under the cyclic thermo-mechanical loading are presented in Sec. 4. Section 5 provides comprehensive parametric studies with geometry effects and variations of loading condition. Finally, Sec. 6 concludes this paper by summarizing results of this research.

Contributed by the Pressure Vessel and Piping Division of ASME for publication in the Journal of Pressure Vessel Technology. Manuscript received January 30, 2019; final manuscript received March 23, 2019; published online November 27, 2019. Assoc. Editor: Yun-Jae Kim.

## 2 Numerical Procedures

**2.1 Overview of Linear Matching Method.** The LMM is a direct method and numerical procedures for calculating shakedown and ratchet limits. It is a flexible and versatile method with the distinctive features that provide compatible results at each stage of the analysis, incorporates detailed ratchet analysis [20,21] and includes temperature dependent material property effects. The LMM determines nonlinear elastic–plastic material response and limit state solutions through a series of linear elastic finite element analysis solutions, in which the local elastic modulus is modified based on the previous solution. Repeating the linear analysis with the updated modulus develops stress redistributions over the structure. This process repeats until the equivalent stress levels match the material yield stress, obtaining accurate load multipliers for upper bound and lower bound to limit load, shakedown, and ratchet limits. The material is assumed to have the elastic perfectly plastic (EPP) and to satisfy plastic incompressibility and the von-Mises yield criterion. The shakedown and the ratchet theorem are summarized briefly in Secs. 2.2 and 2.3.

**2.2 Shakedown Theorem.** The shakedown response has constant residual stress $\rho_{ij}^r$, which can be described by the range of a load multiplier $\lambda$, which should satisfy $\lambda \le \lambda_s$, where $\lambda_s$ denotes the shakedown limit. The LMM calculates both the lower and upper bound limits for the shakedown range.

In the lower bound shakedown theorem of Melan [22], the following condition should be satisfied within the fixed residual stress field $\bar{\rho}$ to keep maintain a state of stress over a structure

$$f(\lambda_{\mathrm{LB}}^{\mathrm{SD}}\hat{\sigma}_{ij} + \bar{\rho}_{ij}) \le 0\,, \text{ then } \lambda_{\mathrm{LB}}^{\mathrm{SD}} \le \lambda_s \tag{1}$$

where $\lambda_{\mathrm{LB}}^{\mathrm{SD}}$ is a shakedown lower bound multiplier and $\hat{\sigma}_{ij}$ is an induced elastic solution. This repeats the iterative process until satisfying Eq. (1), calculating the shakedown lower bound multiplier.

The upper bound shakedown theorem of Koiter is that the upper bound multiplier $\lambda_{\mathrm{UB}}^{\mathrm{SD}}$ should be greater than 1.0 for all kinematically admissible strain rate histories $(\Delta\varepsilon_{ij}^k = \int_0^{\Delta t} \dot{\varepsilon}_{ij}^k dt)$ over an independent time period $\Delta t$. Hence, the following condition should be satisfied:

$$\lambda_{\mathrm{UB}}^{\mathrm{SD}} \int\int_{V0}^{t} \hat{\sigma}_{ij}(x,t)\dot{\varepsilon}_{ij}^k(x,t)dtdV = \int\int_{V0}^{t} D(\dot{\varepsilon}_{ij})dtdV\,, \text{ then } \lambda_{\mathrm{UB}}^{\mathrm{SD}} \ge \lambda_s \tag{2}$$

where $V$ is a 3D body of volume and $D$ is a dissipation of energy during plastic deformation.

Considering a structure with surface area $S$, and volume $V$ and an elastic perfectly plastic material satisfying von-Mises yield criterion, part of $S$ is subjected to cyclic loading (mechanical/thermal) and constant loading (mechanical/thermal) within $V$ for a cyclic time period $\Delta t$. The remaining part of surface $S$ has zero displacement rates. Based on the upper bound theorem, the admissible strain rate history is associated with a displacement increment field; therefore, the shakedown upper bound multiplier can be defined for the combined load history by

$$\lambda_{\mathrm{UB}}^{\mathrm{SD}} \int\int_{V0}^{t} \hat{\sigma}_{ij}(x,t)\dot{\varepsilon}_{ij}^k(x,t)dtdV = \int\int_{V0}^{t} \sigma_{ij}^k \dot{\varepsilon}_{ij}^k dtdV \tag{3}$$

$$\lambda_{\mathrm{UB}}^{\mathrm{SD}} = \frac{\int_0^V \int_0^{\Delta t} \sigma_y \bar{\dot{\varepsilon}}\left(\dot{\varepsilon}_{ij}^k\right) dtdV}{\int_0^V \int_0^{\Delta t} \left(\hat{\sigma}_{ij}\dot{\varepsilon}_{ij}^k\right) dtdV} \tag{4}$$

where $\sigma_{ij}^k$ is a stress state in associated with $\dot{\varepsilon}_{ij}^k$ at yield stress $\sigma_y$ and $\bar{\dot{\varepsilon}}$ is the effective strain rate $\bar{\dot{\varepsilon}} = \sqrt{(2/3)\dot{\varepsilon}_{ij}\dot{\varepsilon}_{ij}}$. The upper bound multiplier is calculated when the least multiplier is satisfied by $\lambda_{\mathrm{UB}}^{\mathrm{SD}} \ge \lambda_s$.

**2.3 Ratchet Theorem.** The ratchet limit is the load limit that lies in between where accumulated plastic strain does not increase over a cycle and where accumulated plastic strain causes incremental failure. The ratchet limit can be obtained numerically by adopting a two-step procedure within the LMM framework. First, the residual stress $\rho_{ij}^r$ and corresponding plastic strain range are calculated by incremental minimization of the energy function $I(\dot{\varepsilon}_{ij}^k, \lambda)$ for a predefined cyclic load

$$I(\dot{\varepsilon}_{ij}^k, \lambda) = \int_V \int_0^{\Delta t} (\sigma_{ij}^k - \sigma_{ij})\dot{\varepsilon}_{ij}^k dtdV \tag{5}$$

where $\sigma_{ij}^k$ denotes yield stress corresponding to the kinematically admissible strain rate $\dot{\varepsilon}_{ij}^k$.

Second, the ratchet limit is computed by performing a global minimization of the shakedown theorem with respect to an extra constant load $\hat{\sigma}_{ij}^F$ where the varying residual stress $\rho_{ij}^r(x,t)$ at a steady cycle enhances the cyclic elastic solution. Hence the cyclic elastic solution for ratchet limit analysis can be defined by

$$\hat{\sigma}_{ij} = \lambda\hat{\sigma}_{ij}^F + \hat{\sigma}_{ij}^{\Delta}(x,t) + \rho_{ij}^r(x,t) \tag{6}$$

where $\hat{\sigma}_{ij}^{\Delta}(x,t)$ is an elastic solution with constant residual stress $\bar{\rho}_{ij}^r$.

Direct steady cycle analysis in the LMM framework calculates the accumulated residual stress history. Direct steady cycle analysis repeats cycles from $m=1$ to $m=M$. The each cycle $m$ has subcycles that represent the load instances from $k=1$ to $k=K$. The constant residual stress $\bar{\rho}_{ij}^r$ and varying residual stress $\Delta\rho_{ij}^r$ corresponding to the elastic solution can be calculated as the following equations:

$$\bar{\rho}_{ij}^r = \sum_{m=1}^{M}\sum_{k=1}^{K} \Delta\rho_{ij}^r(x,t_k)_m \tag{7}$$

$$\rho_{ij}^r(x,t_k) = \bar{\rho}_{ij}^r(x) + \sum_{l=1}^{k} \Delta\rho_{ij}^r(x,t_l)_M \tag{8}$$

The converged plastic strain developed at a time $t_k$ can be expressed as

$$\Delta\varepsilon_{ij}^p(x,t_k) = \frac{1}{2\bar{\mu}_n(x,t_k)}\left[\hat{\sigma}_{ij}^{\Delta'}(x,t_k) + \rho_{ij}^{r'}(x,t_k)\right] \tag{9}$$

where $\bar{\mu}$ is the iterative shear modulus calculated by the LMM and (') indicates deviatoric stress and strain.

Adopting the von-Mises yield criterion for an elastic perfectly plastic material, the upper bound multiplier $\lambda_{\mathrm{UB}}^{\mathrm{RC}}$ for the ratchet limit can be defined by

$$\lambda_{\mathrm{UB}}^{\mathrm{RC}} = \frac{\int_V \sum_{k=1}^{K} \sigma_y \bar{\varepsilon}\left(\Delta\varepsilon_{ij}^k\right) dV - \int_V \sum_{k=1}^{K} \left[\hat{\sigma}_{ij}^{\Delta}(t_k) + \rho_{ij}^r(t_k)\right]\Delta\varepsilon_{ij}^k dV}{\int_V \hat{\sigma}_{ij}^F\left(\sum_{k=1}^{K}\Delta\varepsilon_{ij}^k\right) dV} \tag{10}$$

where $\bar{\varepsilon}$ is the effective strain $\bar{\varepsilon}(\Delta\varepsilon_{ij}^k) = \sqrt{(2/3)\Delta\varepsilon_{ij}^k\Delta\varepsilon_{ij}^k}$. Based on this iterative procedure, the LMM calculates the least upper bound limit for the ratchet limit.

In the case of the lower bound multiplier $\lambda_{\mathrm{LB}}^{\mathrm{RC}}$ for the ratchet limit, the constant residual stress is taken into account

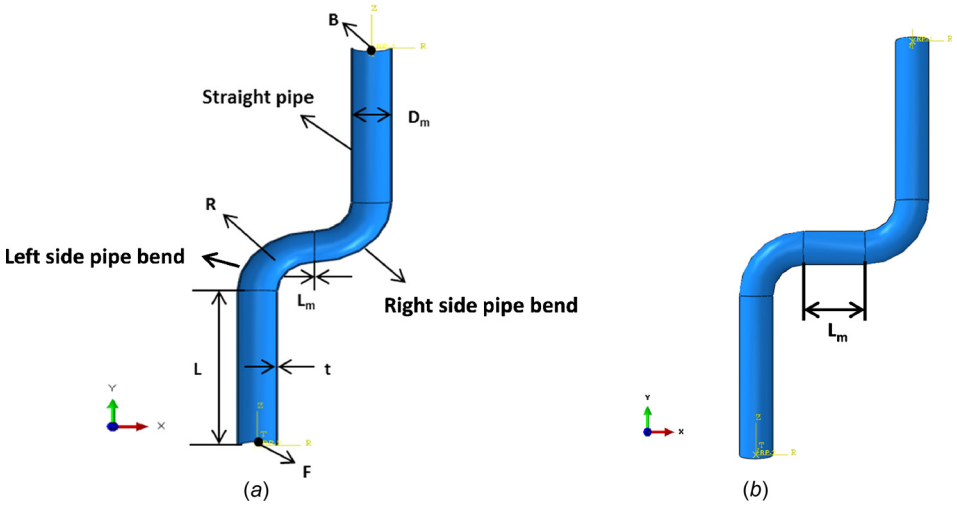


**Fig. 1 The geometry of the pipe configuration with the horizontal straight pipe sections: (*a*) $L_m = 0.0$ mm and (*b*) $L_m = 500.0$ mm**

simultaneously with the varying residual stress field at every iterative process. Thus, the lower bound multiplier can be defined by modifying Eq. (1) with Eq. (6)

$$f(\lambda_{\mathrm{LB}}^{\mathrm{RC}}\hat{\sigma}_{ij}^{F} + \hat{\sigma}_{ij}^{\Delta} + \rho_{ij}^{r}) \leq 0 \tag{11}$$

## 3 Problem Descriptions

**3.1 The Pipe Bend Model.** Two pipe system configurations are investigated, one with two directly connected pipe bends and one in which the bends are connected by a horizontal straight pipe section. Both pipe arrangements are shown in Fig. 1. One without the horizontal pipe is the main geometry for this analysis, whereas the other one is used only for parametric studies. The pipe dimensions conform to U.S. standard pipe size 10 in. NPS Schedule 40. The mean pipe diameter is $D_m$, the straight end runs are length $L$ and the bend connecting run length is $L_m$. It is considered that the pipe bend system can be defined as two ratios: $r/t$ and $R/r$, where $r$ is the mean radius of the pipe; $t$ is the wall thickness of the pipe; $R$ is the bend radius. Dimensions of the configuration are summarized in Table 1. The pipe bend behavior is generally described in terms of these ratios and the pipe bend parameter or pipe factor $h$

$$h = \frac{Rt}{r^2} = \frac{R/r}{r/t} \tag{12}$$

Complete 3D finite element models of the configurations in ABAQUS using 3D solid C3D20R quadratic elements, as shown in Fig. 2. Following a mesh refinement study, the configuration of the main pipe system has meshed with 13,800 elements. Three elements are defined through the wall thickness. Each pipe bend has 25 elements along its length and 50 around its circumference. The vertical straight runs $L$ has meshed with 50 elements with the mesh refined toward the intersection with the pipe bend.

**3.2 Material Properties and Boundary Conditions.** The material investigated is type 304 stainless steel, previously considered in Ref. [18]. Young's modulus is 193.74 GPa and Poisson's ratio is 0.2642. Temperature-dependent yield stresses up to 550 °C are listed in Table 2 and the material model is elastic perfectly plastic.

As shown in Fig. 1, a reference node is created on both the bottom and top of the pipe system: F for the bottom and *B* for the top of the pipe system. The kinematic coupling is constructed between each reference node and whole surfaces of the pipe system in the same $x$–$z$ plane and it allows the expansion/contraction in the radial direction.

Figure 3 illustrates a loading pattern of the cyclic bending moment and the thermal gradient over the pipe system configuration. The cyclic thermal load is implemented by applying the temperature difference between the external and internal surfaces of the pipe system as shown in Fig. 3(*b*). For the cyclic thermal loading, the most severe thermal loading condition during "start-up" is applied as a through wall thermal gradient with the temperature 550 °C at the inside surface and 20 °C at the outside surface, so that. The material is assumed to have a thermal conductivity

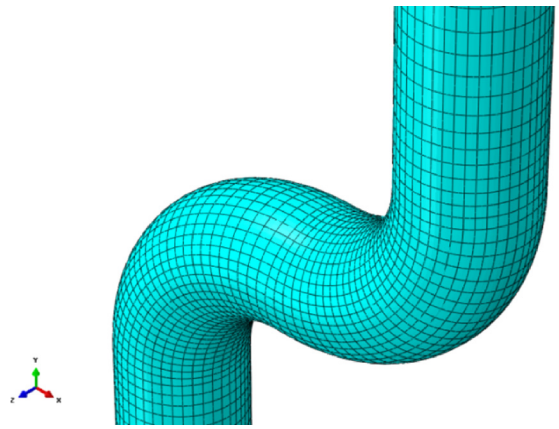

**Fig. 2 The meshed model with 3D solid elements**

**Table 1 Pipe bend dimensions and the two straight pipes (mm)**

| $D_m$ | $R$ | $t$ | $L = 5D_m$ | $r/t$ | $R/r$ |
|---|---|---|---|---|---|
| 263.78 | 381 | 9.27 | 1318.9 | 14.23 | 2.89 |

**Table 2 Temperature dependent yield stress**

| Temperature (°C) | 20 | 100 | 200 | 300 | 400 | 500 | 550 |
|---|---|---|---|---|---|---|---|
| $\sigma_y$(MPa) | 271.93 | 253 | 229 | 207 | 188 | 172 | 156 |

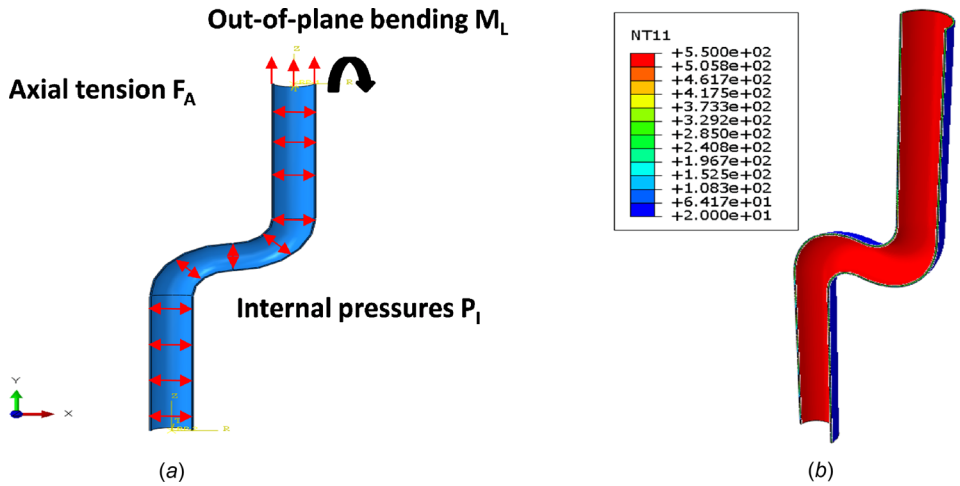


**Fig. 3 (*a*) configuration of the bending and internal pressures and (*b*) thermal gradient through a wall thickness**

of $43\,\mathrm{Wm}^{-1}\,\mathrm{K}^{-1}$ and the thermal expansion coefficient of $1.7 \times 10^{-5}\,^{\circ}\mathrm{C}^{-1}$. By applying an equation to constrain the top surface of the right side vertical pipe as a plane condition, the thermal expansion effect of a long pipe is achieved.

To implement the cyclic out-of-plane bending, a clockwise moment about the $x$-axis is applied on node B. An analytic equation to calculate the limit moment $M_L$ is used for the normalization of the computed moment value as given by the following equation:

$$M_L = \sigma_y D_m^2 t \tag{13}$$

The internal surfaces of pipe configuration have constant pressures. It is assumed that the pipe bends are in a closed-end condition, which generates the axial tension on the top side of the pipe system proportionally to the internal pressure. Analytic equations are employed to normalize the internal pressure and axial tension, as given in the following equation:

$$P_L = \frac{2}{\sqrt{3}}\left(2\sigma_y t/D_m\right) \tag{14}$$

$$F_A = P_L D_m/4t \tag{15}$$

where $P_L$ is the limit pressure; $F_A$ is the axial tension.

Loading paths between the cyclic out-of-plane bending and constant pressure (*loading type* A), cyclic out-of-plane bending and cyclic thermal load (loading type B), and cyclic thermal load and constant pressure (*loading type* C) conform to the classic Bree problem. A cuboid loading domain for the three load combinations is considered to present a shakedown limit domain of the pipe bends in a three-dimensional loading space. The loading paths and the loading domain are illustrated in Fig. 4.

## 4 Cyclic Thermo-Mechanical Loading and Constant Internal Pressure

Figure 5 shows three linear elastic solutions of the pipe system under the three individual loads: thermal loading, out-of-plane bending, and internal pressure. The thermal load produces the maximum tensile stress at the outside of the pipe structure but the compressive stress at the inside due to the nonisothermal effects. The thermal expansion coefficient of the material is a critical factor that leads to these thermal stresses. The bending moment causes the clockwise overturning moment to the pipe bend so that the flank of the left side pipe bend has the maximum equivalent stress. The internal pressures cause the anticlockwise moment to

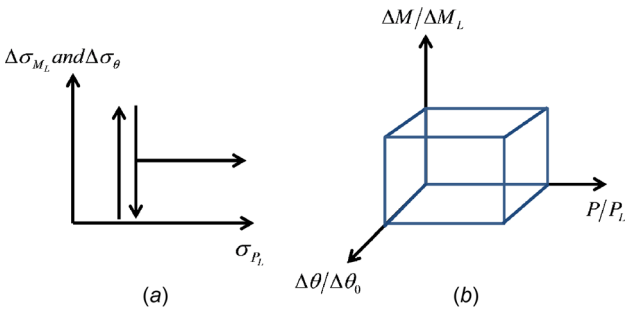


**Fig. 4 (*a*) Loading paths for the three loading types A–C and (*b*) a loading domain for the three load combinations**

the pipe bend so that the intrados of the left side pipe bend has the maximum equivalent stress. Among the three different loads, the maximum equivalent stress value is in order of out-of-plane bending, thermal load, and constant pressure.

The cyclic plastic analysis is performed by the LMM for the pipe system subjected to the three load cases defined as loading type A, loading type B, and loading type C in Sec. 3.2. The shakedown and ratchet limit boundaries under the three load types are presented in Fig. 6(*a*). Figure 6(*b*) illustrates a shakedown limit domain of the pipe structure in a three-dimensional loading space shown in Fig. 4(*b*).

**4.1 Case 1: Loading Type A.** The limit pressure and limit moment of the pipe configuration under loading type A reduces to 76% and 53%, respectively, against the reference pressure and bending moment. We can see that the out-of-plane bending makes more critical impacts on the load bearing capacity of the pipe system than the constant pressures.

The normalized shakedown limit without any pressure applied is called the reverse plasticity limit. For cyclic loading beyond this limit, a certain range of plastic deformation develops as a closed loop until it reaches the ratchet limit. The normalized limit load, shakedown and ratchet limits without any bending moment is known as the limit pressure. For cyclic loading exceeding this limit, the structural failure occurs immediately. One interesting point associated with the shakedown limit boundary under cyclic out-of-plane bending is that the reverse plasticity limit is almost the same as the normalized limit moment. Therefore, the shakedown limit boundary for $P/P_L < 0.4$ is almost indistinguishable from the ratchet limit boundary. There are some margins appeared for $P/P_L > 0.4$ but hard to define the ratchet limit boundary.

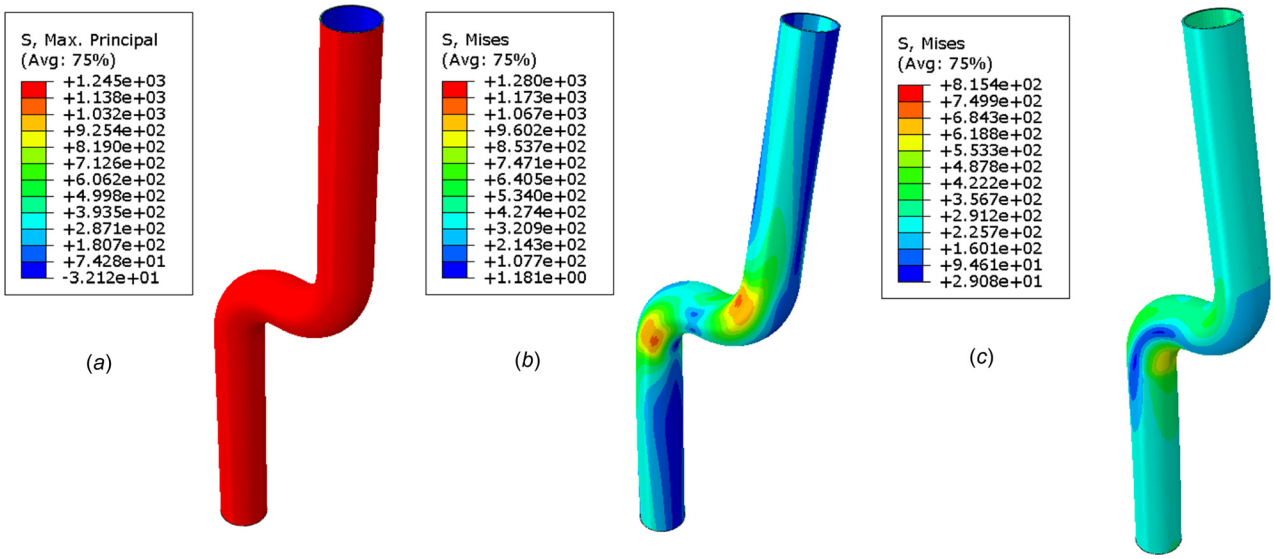


**Fig. 5 Linear elastic solutions: (*a*) maximum principal stress (MPa) under thermal load, (*b*) equivalent stress (MPa) under out-of-plane bending moment, and (*c*) equivalent stress (MPa) under internal pressures**

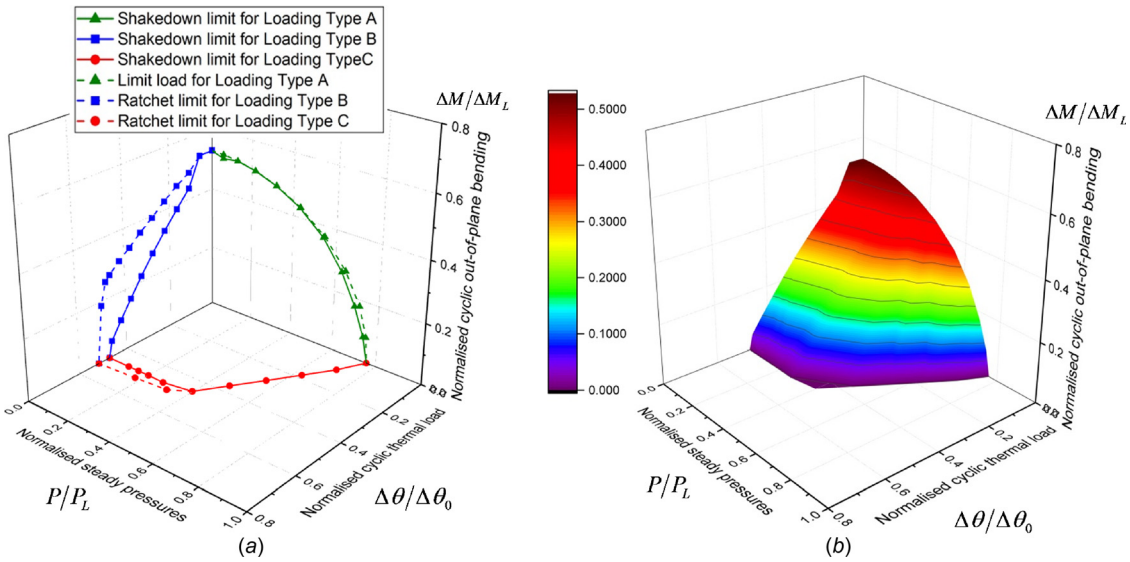


**Fig. 6 (*a*) Shakedown and ratchet limit boundaries of the pipe system subjected to cyclic thermal load, cyclic out-of-plane bending and constant internal pressure and (*b*) shakedown domain in the three-dimensional loading space**

Upon the case, we need to consider the shakedown limit boundary is the same as the ratchet limit boundary as a conservative manner. It is noteworthy that the previous study [18] shows that the pipe system under cyclic in-plane bending has a completely different shape of the shakedown limit boundary from the one under cyclic out-of-plane bending. The cyclic in-plane bending produced the boundary which is very similar to Bree-like diagram with large margins between the limit load and the shakedown boundaries. Therefore, the effects of the bending direction on the cyclic plasticity of the concerned pipe system configuration need to be considered when designing the allowable load level.

**4.2 Case 2: Loading Type B.** When it comes to the ratchet limit boundary, the pipe bend structure can withstand the loading at 53% under cyclic out-of-plane bending and 54% under cyclic thermal load, compared to their reference bending moment and temperature, respectively. Regarding the reverse plasticity limit, the normalized value by the cyclic thermal load is almost the same as by the cyclic out-of-plane bending. Hence, the effects of cyclic thermal load on the pipeline integrity require serious considerations.

Different from the shape of the shakedown limit boundary under loading type A, loading type B develops a shakedown limit boundary of a triangular shape which merges to the reverse plasticity limit of cyclic out-of-plane bending for $\Delta M/\Delta M_L > 0.5$. Hence, the ratchet limit under loading type B should be considered as the shakedown limit boundary where $\Delta M/\Delta M_L > 0.5$. However, the margin between the ratchet limit boundary and the shakedown limit boundary becomes larger as the cyclic thermal load increases up to the reverse plasticity limit of cyclic thermal load, $\Delta\theta/\Delta\theta_0 = 0.54$. It is noteworthy that the thermal ratcheting does not occur in the Bree problem under the pure cyclic thermal load, but it does in the double pipe bend structure where $\Delta\theta/\Delta\theta_0 > 0.54$. Therefore, the allowable load level should be selected from below the shakedown limit boundary.

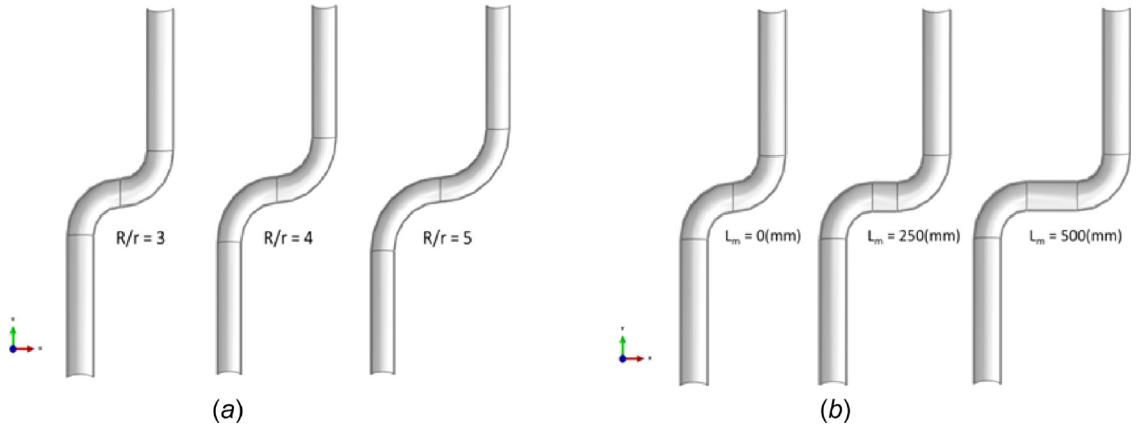


**Fig. 7 (*a*) *R/r* ratio 3, 4, 5 and (*b*) horizontal pipe length $L_m = 0$ mm, 250 mm, 500 mm**

**Table 3 Reference loads computed for each *r/t* ratio**

| $r/t$ | $F_A$(MPa) | $P_L$(MPa) | $M_L$(Nmm) |
|---|---|---|---|
| 5 | 157 | 62.80 | $4.9 \times 10^8$ |
| 10 | 157 | 31.40 | $2.5 \times 10^8$ |
| 20 | 157 | 15.70 | $1.2 \times 10^8$ |

**4.3 Case 3: Loading Type C.** Shakedown limit boundary under loading type C shows very similar shape to the exemplary Bree diagram. Where $P/P_L < 0.3$, the shakedown limit boundary maintains the constant reverse plasticity limit, and afterward slightly decreases until $P/P_L = 0.4$. The margin that shows the reverse plasticity response is small due to the thermal ratchet limit. Therefore, the proper load level should be selected under the shakedown limit boundary.

## 5 Further Numerical Studies and Discussion

Figure 7 presents the changes in the bend characteristics ($R/r$ and $r/t$) and the horizontal pipe run ($L_m$) of the pipe bend system. In this numerical study, the effects of the varying geometry on the cyclic plasticity will be investigated under cyclic thermal load and cyclic out-of-plane bending, respectively, with constant pressure. The same equations from Eqs. (13) to (15) are employed for the normalization process and the computed reference loads are summarized in Table 3.

**5.1 Cyclic Thermal Load and Constant Internal Pressures.** In this section, the effects of the geometry changes on the cyclic plasticity of the pipe bend under cyclic thermal load and constant internal pressure are investigated. Figure 8 shows a comparison of the shakedown and ratchet limit boundaries for changing $R/r$ ratio against a fixed $r/t = 5$. Internal pressures are normalized by pressures in Table 3 and a reference temperature $\Delta\theta_0 = 550\,^{\circ}\mathrm{C}$ is employed to normalize the cyclic temperature load.

The constructed shakedown limit boundaries have a very similar shape to the typical Bree diagram. The results provide interesting observations that the calculated reverse plasticity limit is the same regardless of changes of $R/r$ ratio. The variations of $R/r$ ratios (3–5) have minor effects on the thermal stress magnitude of the pipe structure. It demonstrates that the reverse plasticity limit reported in Fig. 6(*a*) is also the same as in Fig. 8. Also, Chen et al. presented the effect of cyclic thermal load on a single elbow bend with the varying $R/r$ ratio, it confirms that reverse plasticity limits are very close to each other [16].

Ratchet limit boundaries of $R/r$ ratio of 4 and 5 have the thermal ratchet limit; thus, they have a similar form with a shakedown limit boundary of the Bree diagram. However, no thermal ratchet

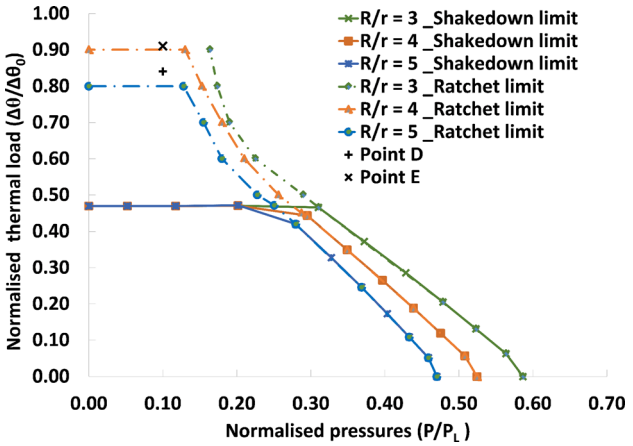


**Fig. 8 Structural response interaction boundaries of the pipe system (*r/t* = 5) subjected to cyclic thermal load and constant internal pressure against variations of *R/r* ratio**

limit is observed for $R/r = 3$ below the normalized thermal load of 1.0. In Fig. 8, two cyclic loading points D ($\Delta\theta/\Delta\theta_0 = 0.85$ and $P/P_L = 0.1$) and E ($\Delta\theta/\Delta\theta_0 = 0.92$ and $P/P_L = 0.1$) are created to validate the ratchet limit boundary of $R/r$ ratio of 4 and 5. The full incremental cyclic analysis is performed to evaluate the plastic strain increment over a number of load instances. As the results of the validation, Fig. 9 shows the clear ratcheting response which appears in the $R/r$ ratio of 4 and 5, whereas $R/r$ ratio 3 exhibits no ratcheting response but alternating plasticity. From the results, we can see that the higher temperature field affects pipe bends and the reverse plasticity zone becomes smaller as the $R/r$ ratio increases. The cyclic thermal load affects ratchet limit boundary but merely shakedown limit boundary for variations of $R/r$ ratio.

Further study is performed for investigating shakedown limit boundaries of the same pipe structure subjected to the cyclic thermal load, constant internal pressure, and constant out-of-plane bending. The same reference pressure and temperature are adopted for the normalization. Figure 10 depicts the resulting shakedown limit boundaries with variations of $R/r$ ratio (3–5) against a fixed $r/t = 5$. Although the constant out-of-plane bending moment is applied together with the pressure, the shape of shakedown limit boundaries is similar to the Bree diagram. The reverse plasticity limits do not change for $P/P_L \& M/M_L < 0.2$, regardless of the variation of $R/r$ ratio, but the combined constant pressure and bending moment are reduced to 11%, 7%, and 5%, respectively, as $R/r$ ratio increases 3–5. Therefore, it is deduced that the geometry changes under cyclic thermal load and constant pressure (or combined with the bending moment) have minor

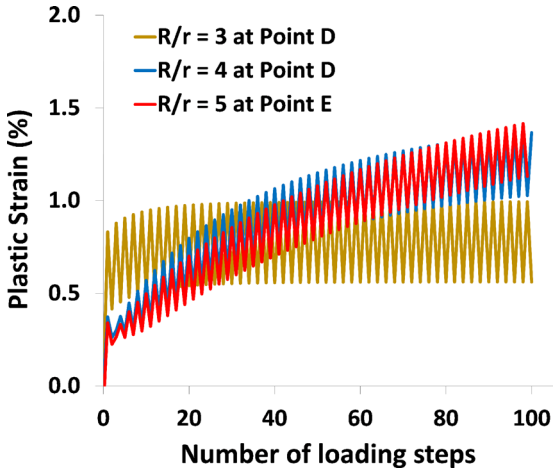


**Fig. 9 Plastic strain history (PEMAG) of *R/r* ratio 3 and 4 at cyclic loading point D and of *R/r* ratio 5 at cyclic loading point E**

effects on the shakedown limit boundaries but considerable impacts on thermal ratchet limit.

### 5.2 Cyclic Out-of-Plane Bending and Constant Internal Pressures

*5.2.1 Geometry Effects of the Pipe Bend Characteristics.* In this section, the effects of changing $R/r$ ratios (3–5) on the cyclic plasticity of the pipe bend ($r/t = 5$, 10, and 20) under cyclic out-of-plane bending and constant internal pressure are investigated. Figure 11 shows structural response interaction boundaries under the geometry changes, where LM curve is the limit load boundary and SD & RC curves are the shakedown limit and the ratchet boundary, respectively. Table 1 shows the other geometries which are the vertical straight pipe $L$ and the mean diameter of $D_m$.

From the results, the normalized limit moment and the reverse plasticity limit at zero pressures are very close to each other. It means that the changes in geometry seldom affect the reverse plasticity limit under cyclic out-of-plane bending. Besides, as $r/t$ ratio decreases, the reverse plasticity limit is likely to enhance but the limit pressure reduces. Thus, the pipe system with larger $R/r$ ratio has higher endurance against the cyclic out-of-plane bending, but lower endurance against the internal pressure.

In the case of $r/t = 5$ (thick-walled), shakedown limit boundaries for $P/P_L < 0.3$ are equal to corresponding limit load boundaries. The margins between the limit load and shakedown limit

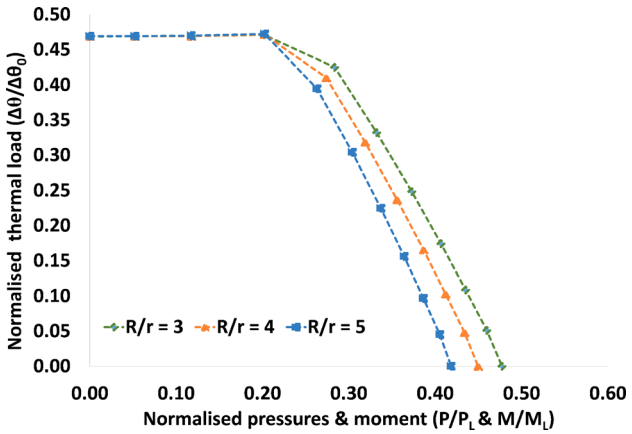


**Fig. 10 Structural response interaction boundaries of the pipe system under the constant out-of-plane bending, constant internal pressure, and cyclic thermal load against variations of *R/r* ratio**

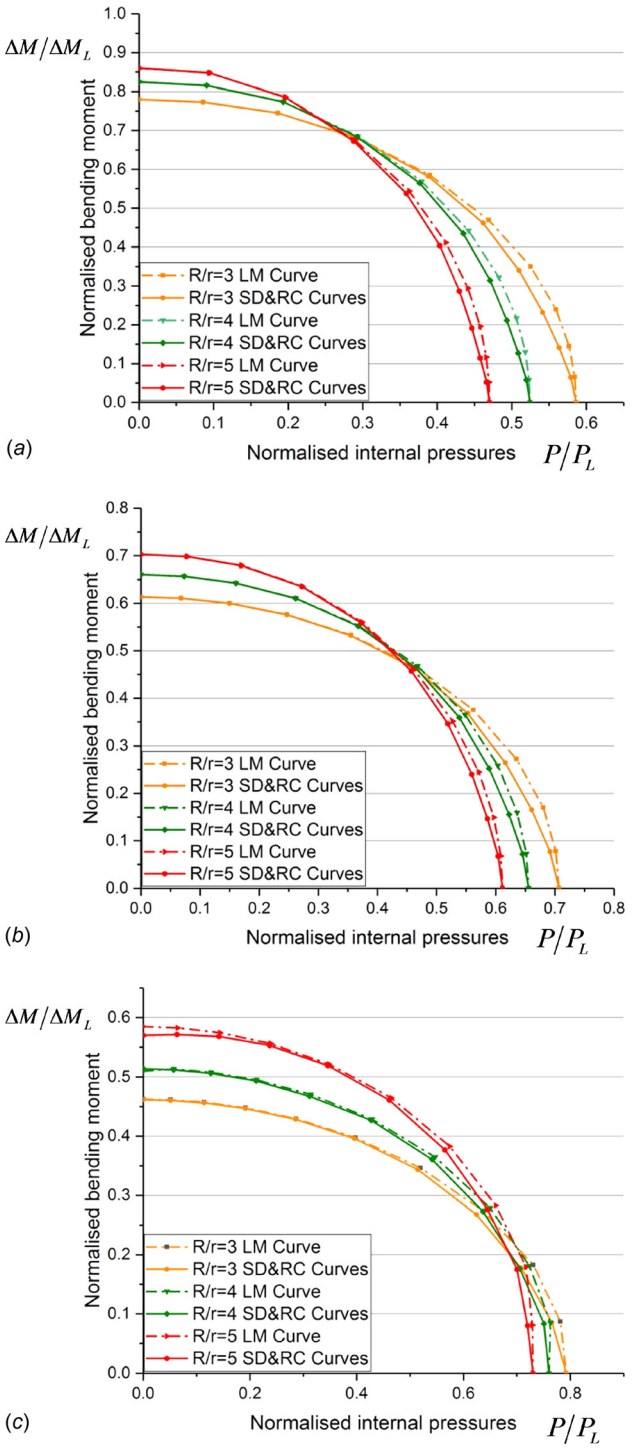


**Fig. 11 Structural response interaction boundaries of the pipe system under the effects of *R/r* ratio: (*a*) *r/t* = 5, (*b*) *r/t* = 10, and (*c*) *r/t* = 20**

boundaries begin to form where $P/P_L > 0.3$ but they are small. Although the margins slightly increase by increasing of $R/r$ ratio, the ratchet limit boundary is too small to be constructed. Hence it is recommended that the shakedown limit boundary should be dealt with the ratchet limit boundary. The thick-walled pipe has lower endurance capacity against the constant pressures than the cyclic out-of-plane bending. With increasing of $R/r$ ratio, the limit moment and reverse plasticity limit increase for $P/P_L < 0.3$, but decrease for $P/P_L > 0.3$. Compared to the previous study [18], cyclic out-of-plane bending generates a larger elastic

shakedown limit boundary but smaller reverse plasticity zone. Therefore, the thick-walled application is an appropriate design for a piping network operated under a high level of cyclic out-of-plane bending.

In the case of $r/t = 10$ and $r/t = 20$ (thin-walled), the shakedown limit boundaries are also very adjacent to limit load boundaries. They have very small margins for each $R/r$ ratio so that the shakedown limit boundary can replace to ratchet limit boundary. With an increase of $r/t$ ratio, the limit pressure decrease but the reverse plasticity limit increases. With an increase of $R/r$ ratio, the pipe system with $r/t = 10$ has higher resistance to the bending for $P/P_L < 0.45$ but reduces for $P/P_L > 0.45$. The pipe system with $r/t = 20$ shows the higher bending resistance for $P/P_L < 0.68$, whereas lower bending resistance for $P/P_L > 0.68$. Compared to the previous study, reverse plasticity limits for $r/t = 20$ are higher under cyclic out-of-plane bending than cyclic in-plane bending. Therefore, we can expect that the pipe bends have higher endurance capacity against cyclic bending moments in the out-of-plane direction than the in-plane direction.

The previous study [18] derived the relationships between reverse plasticity limit $RP_{\text{lim}}^{\text{in-plane}}$ and the bend characteristic $h$ and between limit pressures $LP_{\text{lim}}^{\text{in-plane}}$ and the bend characteristic $h$ as in the following equations:

$$RP_{\text{lim}}^{\text{in-plane}} = -0.784h^2 + 1.6242h + 0.0492 \tag{16}$$

$$LP_{\text{lim}}^{\text{in-plane}} = 0.2247h^2 - 0.6233h + 0.8751 \tag{17}$$

From the numerical results in Fig. 11, we develop another relationship between the bend characteristic $h$ and reverse plasticity limit $RP_{\text{lim}}^{\text{out-of-plane}}$ and between the bend characteristic $h$ and a ratio ($RT = \frac{RP_{\text{lim}}^{\text{out-of-plane}}}{RP_{\text{lim}}^{\text{in-plane}}}$) and by adopting the Quadratic Regression method as given in the following equations:

$$RP_{\text{lim}}^{\text{out-of-plane}} = -0.5032h^2 + 1.0227h + 0.3367 \tag{18}$$

$$RT = 1.4312h^2 - 2.3624h + 1.9154 \tag{19}$$

Trends for the newly derived equations are illustrated in Fig. 12 and $R$-squared value of the all equations from Eqs. (16) to (19) are higher than 0.98.

The developed semi-empirical equations can aid a piping system designer to estimate the reverse plasticity limit and limit pressures of the pipe system against varying geometry effects under both in-plane and out-of-plane bending moments, without performing the FE analysis.

*5.2.2 Geometry Effects of the Horizontal Straight Pipe.* In this section, the effects of changing length of the horizontal straight pipe (0, 250, 500 mm) on the cyclic plasticity of the pipe system ($r/t = 5$, 10, and 20 and $R/r = 2.89$) under cyclic out-of-plane bending and constant internal pressure are investigated. Figure 13 presents structural response interaction boundaries under the horizontal length changes. Table 1 shows the other geometries which are the vertical straight pipe $L$ and the mean diameter of $D_m$.

From the results, we observe that limit pressures increase but reverse plasticity limit decreases as the length $L_m$ decrease. However, the variation of the reverse plasticity limit is very small. Under the cyclic out-of-plane bending, the reverse plasticity limits are very close to their corresponding limit moments at zero pressure, which means changes of the horizontal length have no effects on the size of the alternating plasticity zone which is referred to the margin. Owing to small margins between limit load and shakedown limit boundaries, the ratchet limit boundary should be replaced to the shakedown limit boundary. Contrary to the effects of the horizontal pipe length under cyclic in-plane bending [18], the horizontal pipe length under cyclic out-of-plane bending has minor effects on the reverse plasticity limit but significant impacts on the limit pressures.

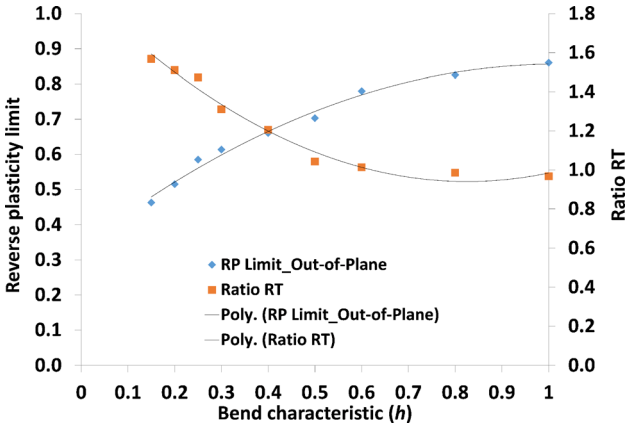


**Fig. 12 Derived relationships from Eqs. (18) and (19)**

In the case of $r/t = 5$ (thick-walled), regardless of the length of $L_m$, we can see the reverse plasticity limit is identical to the normalized limit moment. However, limit pressures decrease with increasing of the length $L_m$. The margins between the limit load and the shakedown limit boundaries appear where $P/P_y > 0.2$ but very minimal. In terms of the endurance, the pipe system with $r/t = 5$ has larger normalized moment values than normalized pressure values despite the existence of horizontal pipe length. Thus, the thick-walled pipe with the horizontal pipe runs is a suitable application for a high level of cyclic out-of-plane bending expected during operations.

In the case of $r/t = 10$ and $r/t = 20$ (thin-walled), reverse plasticity limits and normalized limit moment values at zero pressures are nearly equal. The maximum change in the reverse plasticity limit between each horizontal length is 0.1. The limit pressure decreases as the length $L_m$ increases. The margins appears at where $P/P_y > 0.26$ and $P/P_y > 0.39$, respectively, but still too narrow to construct the ratchet limit boundaries. Compared to the previous study, the pipe systems have a greater bending resistance of 15% and 20%, respectively. It observed that changes in the horizontal straight pipe length make less impact on the reverse plasticity limit but effective on internal pressures. In particular, the pipe structure of $r/t = 5$ with $L_m = 500$ mm has over 20% pressure reduction from the pipe structure without the horizontal pipe. Therefore, the horizontal pipe length should be designed as short as possible if thick walled pipe bends subjected to high internal pressure operation.

These studies show the effects of the horizontal pipe length on the integrity of the pipe structure, which makes significant impacts on the constant pressures but negligible impacts on the cyclic out-of-plane bending. Due to the small margins, plastic collapse can occur if operational loading beyond the elastic shakedown limit boundary.

## 6 Conclusions

Cyclic plasticity of the 90-deg back-to-back pipe bend structure subjected to cyclic thermo-mechanical loading is investigated by means of the LMM. With the observed results, following conclusions and remarks are made:

- With thermal load effects, the pipe bend structure under cyclic thermal load shows almost the same reverse plasticity limit as the structure subjected to cyclic out-of-plane bending. Therefore, the thermal stress effects require serious consideration of the integrity assessment of the pipe bends structure. Moreover, this study demonstrates that geometry changes such as variations of $r/t$ and $R/r$ ratios do not affect reverse plasticity limit of the pipe bends under the cyclic

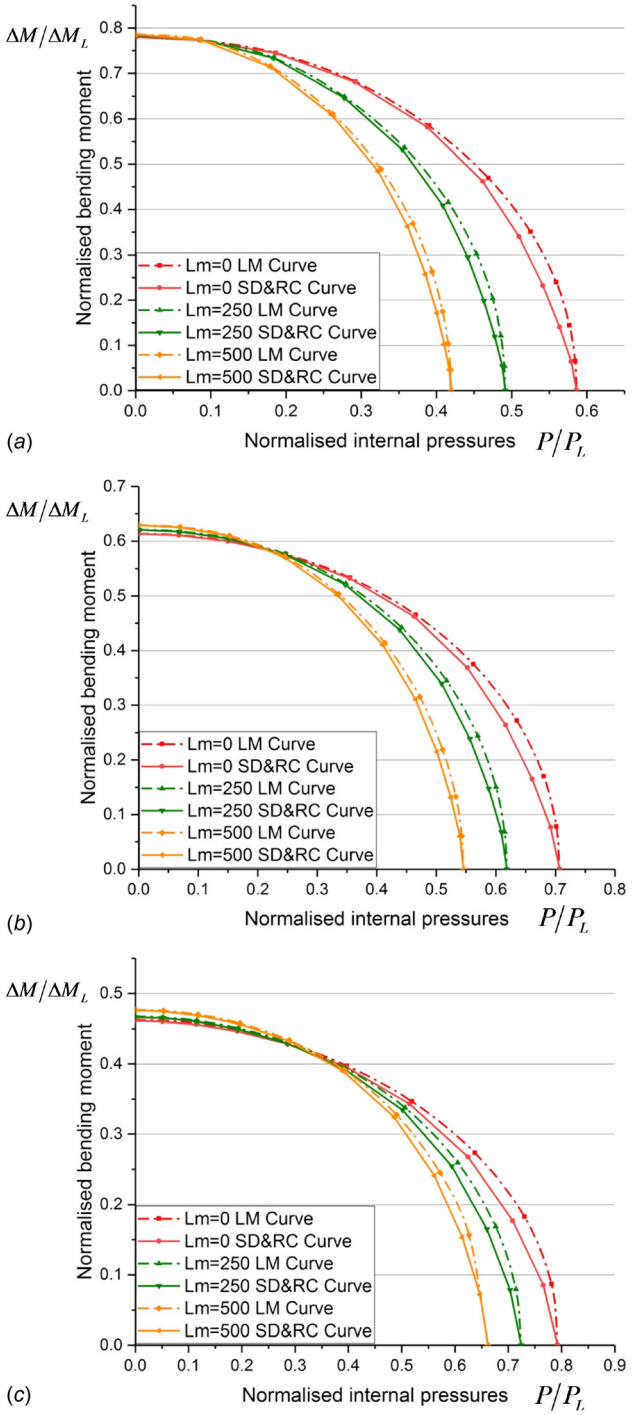


**Fig. 13 Structural response interaction boundaries of the pipe system under the effect of the horizontal pipe length $L_m$: (*a*) $r/t = 5$, (*b*) $r/t = 10$, and (*c*) $r/t = 20$**

thermal load, whereas they have significant influences on the reverse plasticity limit under the cyclic bending moments. Utilizing the effect of temperature dependent material properties, this research presents more practical structural response against the complex thermo-mechanical loading.

- Without thermal load, the pipe bend structure under cyclic out-of-plane bending and constant internal pressure show shakedown limit boundary which is very adjacent to limit load boundary regardless the changes in geometry so that the shakedown limit boundary should replace the ratchet limit boundary. Therefore, allowable loading should be selected by maintaining enough margins below the elastic shakedown limit boundary. With decreasing of $r/t$ ratio, the pipe bends has large endurance capacity against cyclic out-of-plane bending than the constant pressure as $R/r$ ratio increases. However, the margins between the limit load and shakedown limit boundaries are very minimal. Therefore, conservative approaches in the design of the allowable loading should be made so that it can avoid unexpected plastic collapse. The horizontal pipe length shows very minor effects on the reverse plasticity limit but makes critical impacts on limit pressures.
- Comprehensive parametric studies provide understandings on cyclic plasticity behavior of the pipe bend structure in associated with geometry effects of the pipe bends under different combinations of the loadings defined. In particular, the semi-empirical equations derived in Sec. 5.2.1 can be utilized to estimate shakedown limit boundary instead of carrying out complicated numerical analysis.

## Acknowledgment

The authors gratefully acknowledge the supports from the National Natural Science Foundation of China (51828501), University of Strathclyde and East China University of Science and Technology during the course of this work.

## Funding Data


- National Natural Science Foundation of China (Grant No. 51828501; Funder ID: 10.13039/501100001809).
- University of Strathclyde (Funder ID: 10.13039/100008078).
- East China University of Science and Technology (Funder ID: 10.13039/501100003021).


## References


[1] Karamanos, S. A., 2016, "Mechanical Behavior of Steel Pipe Bends: An Overview," ASME J. Pressure Vessel Technol., **138**(4), p. 041203.

[2] Ni, J., Zhou, S., Zhang, P., and Li, Y., 2015, "Effect of Pipe Bend Configuration on Guided Waves-Based Defects Detection: An Experimental Study," ASME J. Pressure Vessel Technol., **138**(2), p. 021203.

[3] Vogelaar, B., and Golombok, M., 2017, "Damage Detection Through Pipe Bends," ASME J. Pressure Vessel Technol., **139**(5), p. 051701.

[4] Chen, H., Chen, W., Li, T., and Ure, J., 2012, "On Shakedown, Ratchet and Limit Analyses of Defective Pipeline," ASME J. Pressure Vessel Technol., **134**(1), p. 011202.

[5] Muscat, M., and Mackenzie, D., 2003, "Elastic-Shakedown Analysis of Axisymmetric Nozzles," ASME J. Pressure Vessel Technol., **125**(4), pp. 365–370.

[6] Urabe, Y., Takahashi, K., and Abe, H., 2015, "Low Cycle Fatigue Evaluation of Pipe Bends With Local Wall Thinning Considering Multi-Axial Stress State," ASME J. Pressure Vessel Technol., **137**(4), p. 041404.

[7] Ure, J., Chen, H., and Tipping, D., 2015, "Verification of the Linear Matching Method for Limit and Shakedown Analysis by Comparison With Experiments," ASME J. Pressure Vessel Technol., **137**(3), p. 031003.

[8] Bree, J., 1967, "Elastic-Plastic Behaviour of Thin Tubes Subjected to Internal Pressure and Intermittent High-Heat Fluxes With Application to Fast-Nuclear-Reactor Fuel Elements," J. Strain Anal. Eng. Des., **2**(3), pp. 226–238.

[9] Seshadri, R., 1995, "Inelastic Evaluation of Mechanical and Structural Components Using the Generalized Local Stress Strain Method of Analysis," Nucl. Eng. Des., **153**(2–3), pp. 287–303.

[10] Dhalla, A. K., and Jones, G. L., 1986, "ASME Code Classification of Pipe Stresses: A simplified Elastic Procedure," Int. J. Pressure Vessels Piping, **26**(2), pp. 145–166.

[11] Chen, H., and Ponter, A. R., 2001, "Shakedown and Limit Analyses for 3-D Structures Using the Linear Matching Method," Int. J. Pressure Vessels Piping, **78**(6), pp. 443–451.

[12] Chen, H., and Ponter, A. R., 2006, "Linear Matching Method on the Evaluation of Plastic and Creep Behaviours for Bodies Subjected to Cyclic Thermal and Mechanical Loading," Int. J. Numer. Methods Eng., **68**(1), pp. 13–32.

[13] Chen, H., and Ponter, A. R., 2010, "A Direct Method on the Evaluation of Ratchet Limit," ASME J. Pressure Vessel Technol., **132**(4), p. 041202.

[14] Abdalla, H. F., 2014, "Shakedown Boundary Determination of a 90° Back-to-Back Pipe Bend Subjected to Steady Internal Pressures and Cyclic In-Plane Bending Moments," Int. J. Pressure Vessels Piping, **116**, pp. 1–9.

[15] Abdalla, H. F., 2014, "Shakedown Boundary of a 90–Degree Back–to–Back Pipe Bend Subjected to Steady Internal Pressures and Cyclic Out–of–Plane Bending Moments," ASME Paper No. PVP2014-28214.

[16] Chen, H., Ure, J., Li, T., Chen, W., and Mackenzie, D., 2011, "Shakedown and Limit Analysis of 90 Pipe Bends Under Internal Pressure, Cyclic In-Plane Bending and Cyclic Thermal Loading," Int. J. Pressure Vessels Piping, **88**(5–7), pp. 213–222.
[17] Chen, X., Gao, B., and Chen, G., 2006, "Ratcheting Study of Pressurized Elbows Subjected to Reversed In-Plane Bending," ASME J. Pressure Vessel Technol., **128**(4), pp. 525–532.
[18] Cho, N.-K., and Chen, H., 2017, "Shakedown, Ratchet, and Limit Analyses of 90° Back-to-Back Pipe Bends Under Cyclic In-Plane Opening Bending and Steady Internal Pressure," Eur. J. Mech.-A/Solids, **67**, pp. 231–242.
[19] Oh, C.-S., Kim, Y.-J., and Park, C.-Y., 2008, "Shakedown Limit Loads for Elbows Under Internal Pressure and Cyclic In-Plane Bending," Int. J. Pressure Vessels Piping, **85**(6), pp. 394–405.
[20] Chen, H., and Ponter, A. R., 2001, "A Method for the Evaluation of a Ratchet Limit and the Amplitude of Plastic Strain for Bodies Subjected to Cyclic Loading," Eur. J. Mech.-A/Solids, **20**(4), pp. 555–571.
[21] Ponter, A. R., and Chen, H., 2001, "A Minimum Theorem for Cyclic Load in Excess of Shakedown, With Application to the Evaluation of a Ratchet Limit," Eur. J. Mech.-A/Solids, **20**(4), pp. 539–553.
[22] Melan, E., 1936, *Theorie Statisch Unbestimmter Systeme Aus Ideal-Plastischem Baustoff*, Hölder-Pichler-Tempsky in Komm, Vienna, Austria.